Electronic Supplementary Material (ESI) for Journal of Materials Chemistry C.

Electronic Supporting information

for

On the origin of ferroelectric structural phases in perovskite-like metal-organic formate

Adam Sieradzki[1], Mirosław Mączka[2], Mantas Simenas[3], Jan K. Zaręba[4], Anna Gągor[2], Sergejus Balciunas[3], Martynas Kinka[3], Aneta Ciupa[2], Marcin Nyk[4], Vytautas Samulionis[3], Juras Banys[3], Marian Paluch[5], Sebastian Pawlus[5]*

[1]*Departament of Experimental Physics, Wrocław University of Science and Technology, Wyb.Wyspiańskiego 27, 50-370 Wrocław, Poland.*

[2] *Institute of Low Temperature and Structure Research, Polish Academy of Sciences, Box 1410, 50-950 Wrocław 2, Poland.*

[3]*Faculty of Physics, Vilnius University, Saulėtekio 9, LT-10222 Vilnius, Lithuania.*

[4]*Advanced Materials Engineering and Modelling Group, Faculty of Chemistry, Wroclaw University of Science and Technology, Wyb. Wyspiańskiego 27, 50-370, Wrocław, Poland.*

[5] *Institute of Physics, University of Silesia, ul. Uniwersytecka 4, PL-40-007 Katowice, Poland.*

**Email: adam.sieradzki@pwr.edu.pl*

Table 1. Experimental details

Experiments were carried out on Xcaliburdiffractometer with Mo $K_\alpha$radiationAtlas (CCD) camera. Absorption was corrected for by multi-scan methods, *CrysAlis PRO* 1.171.38.43 (Rigaku Oxford Diffraction, 2015) H-atom parameters were constrained.

	PhaseIII	**PhaseII**
Crystal data		
Chemical formula	$C_4H_{10}N_2O_6Zn$	$C_4H_{10}N_2O_6Zn$
M_r	247.51	247.51
Crystal system, space group	Triclinic, *P*1	Trigonal, *R*3*c*:*H*
Temperature (K)	150	180
a, *b*, *c* (Å)	8.029 (2), 8.027 (2), 8.722 (3)	8.0493 (3), 8.0493 (3), 22.260 (1)
α, β, γ (°)	62.81 (3), 63.22 (3), 59.99 (3)	90, 90, 120
V (Å^3)	414.6 (3)	1249.02 (11)
Z	2	6
μ (mm^{-1})	2.97	2.95
Crystal size (mm)	0.21 × 0.18 × 0.13	0.21 × 0.18 × 0.13
Data collection		
T_{min}, T_{max}	0.814, 1.000	0.790, 1.000
No. of measured, independent and observed [$I > 2\sigma(I)$] reflections	2596, 2596, 2136	3217, 697, 664
R_{int}	0.06	0.026
$(\sin\theta/\lambda)_{max}$ (Å^{-1})	0.693	0.690
Refinement		
$R[F^2 > 2\sigma(F^2)]$, $wR(F^2)$, *S*	0.042, 0.115, 0.97	0.019, 0.048, 1.27
No. of reflections	2596	697
No. of parameters	239	51
No. of restraints	147	9
$\Delta\rho_{max}$, $\Delta\rho_{min}$ (e Å^{-3})	0.91, -1.04	0.29, -0.32
Absolute structure	Refined as three component twin using HKLF5. The BASF parameters are equal to 0.32, 0.31 and 0.37. Inversion twins not involved.	Refined as an inversion twin.
Absolute structure parameter	-	0.50 (5)

Computer programs: *CrysAlis PRO* 1.171.38.43 (Rigaku OD, 2015), *SHELXL2014*/7 (Sheldrick, 2014).

Table 2. Selected geometric parameters (Å, º)

Phase III, 150K			
Zn1—O12	2.083 (5)	O6—C15^{i}	1.222 (8)
Zn1—O9	2.092 (4)	O7—C16^{ii}	1.205 (11)
Zn1—O2	2.099 (7)	O8—C13	1.272 (7)
Zn1—O6	2.098 (5)	O9—C13	1.226 (11)
Zn1—O5	2.119 (7)	O10—C14^{iii}	1.249 (9)
Zn1—O3	2.115 (6)	O11—C17^{iv}	1.243 (11)
Zn2—O4	2.055 (6)	O12—C18^{v}	1.236 (12)

Zn2—O11	2.107 (5)	C14—O10^{vi}	1.249 (9)
Zn2—O10	2.101 (5)	C15—O6^{vii}	1.222 (8)
Zn2—O8	2.109 (6)	C16—O7^{viii}	1.205 (11)
Zn2—O7	2.111 (5)	C17—O11^{ix}	1.243 (11)
Zn2—O1	2.119 (6)	C18—O12^{x}	1.236 (12)
O1—C15	1.266 (9)	N3—N4	1.462 (8)
O2—C17	1.238 (8)	C2—N4	1.428 (14)
O3—C14	1.287 (10)	N1—N2	1.466 (9)
O4—C18	1.273 (8)	N1—C1	1.476 (14)
O5—C16	1.259 (8)		
O12—Zn1—O9	179.0 (3)	O4—Zn2—O1	89.3 (2)
O12—Zn1—O2	89.1 (2)	O11—Zn2—O1	88.0 (2)
O9—Zn1—O2	90.2 (2)	O10—Zn2—O1	177.0 (3)
O12—Zn1—O6	92.0 (2)	O8—Zn2—O1	89.1 (2)
O9—Zn1—O6	87.28 (19)	O7—Zn2—O1	91.00 (19)
O2—Zn1—O6	89.3 (2)	C15—O1—Zn2	124.9 (4)
O12—Zn1—O5	93.2 (2)	C17—O2—Zn1	126.1 (6)
O9—Zn1—O5	87.5 (2)	C14—O3—Zn1	122.9 (4)
O2—Zn1—O5	177.33 (19)	C18—O4—Zn2	127.3 (6)
O6—Zn1—O5	91.8 (2)	C16—O5—Zn1	127.9 (6)
O12—Zn1—O3	88.2 (2)	C15^{i}—O6—Zn1	125.4 (4)
O9—Zn1—O3	92.52 (19)	C16^{ii}—O7—Zn2	125.9 (5)
O2—Zn1—O3	90.2 (2)	C13—O8—Zn2	125.3 (6)
O6—Zn1—O3	179.5 (3)	C13—O9—Zn1	124.9 (5)
O5—Zn1—O3	88.7 (2)	C14^{iii}—O10—Zn2	124.1 (4)
O4—Zn2—O11	90.3 (2)	C17^{iv}—O11—Zn2	123.9 (5)
O4—Zn2—O10	88.2 (2)	C18^{v}—O12—Zn1	123.4 (5)
O11—Zn2—O10	93.65 (19)	O9—C13—O8	125.6 (8)
O4—Zn2—O8	175.88 (18)	O10^{vi}—C14—O3	119.2 (6)
O11—Zn2—O8	93.4 (2)	O6^{vii}—C15—O1	121.8 (6)
O10—Zn2—O8	93.3 (2)	O7^{viii}—C16—O5	128.8 (8)
O4—Zn2—O7	89.2 (2)	O2—C17—O11^{ix}	124.6 (8)
O11—Zn2—O7	178.92 (19)	O12^{x}—C18—O4	128.3 (9)
O10—Zn2—O7	87.31 (19)	C2—N4—N3	116.7 (9)
O8—Zn2—O7	87.0 (2)	N2—N1—C1	115.4 (9)
Phase II, 180K			
N1—C2	1.455 (17)	Zn1—O1^{xi}	2.099 (5)
N1—N2	1.47 (2)	Zn1—O1	2.099 (5)
Zn1—O2^{xi}	2.107 (5)	O1—C1	1.258 (10)
Zn1—O2^{xii}	2.107 (5)	O2—C1^{xiii}	1.244 (10)
Zn1—O2	2.107 (5)	C1—O2^{xiv}	1.244 (10)
Zn1—O1^{xii}	2.099 (5)		
C2—N1—N2	113.7 (18)	O1^{xii}—Zn1—O1^{xi}	92.7 (2)
O2^{xi}—Zn1—O2^{xii}	91.1 (2)	O2^{xi}—Zn1—O1	178.8 (3)
O2^{xi}—Zn1—O2	91.1 (2)	O2^{xii}—Zn1—O1	88.46 (17)

O2^{xii}—Zn1—O2	91.1 (2)	O2—Zn1—O1	87.72 (17)
O2^{xi}—Zn1—O1^{xii}	88.46 (17)	O1^{xii}—Zn1—O1	92.7 (2)
O2^{xii}—Zn1—O1^{xii}	87.72 (17)	O1^{xi}—Zn1—O1	92.7 (2)
O2—Zn1—O1^{xii}	178.8 (3)	C1—O1—Zn1	125.6 (4)
O2^{xi}—Zn1—O1^{xi}	87.72 (17)	C1^{xiii}—O2—Zn1	124.6 (4)
O2^{xii}—Zn1—O1^{xi}	178.8 (3)	O2^{xiv}—C1—O1	124.4 (3)
O2—Zn1—O1^{xi}	88.46 (17)		

Symmetrycode(s): (i) *x*, *y*+1, *z*-1; (ii) *x*, *y*, *z*+1; (iii) *x*+1, *y*, *z*; (iv) *x*+1, *y*-1, *z*; (v) *x*-1, *y*+1, *z*-1; (vi) *x*-1, *y*, *z*; (vii) *x*, *y*-1, *z*+1; (viii) *x*, *y*, *z*-1; (ix) *x*-1, *y*+1, *z*; (x) *x*+1, *y*-1, *z*+1; (xi) -*x*+*y*, -*x*+1, *z*; (xii) -*y*+1, *x*-*y*+1, *z*; (xiii) *x*-1/3, *x*-*y*+1/3, *z*-1/6; (xiv) *x*+1/3, *x*-*y*+2/3, *z*+1/6.

Table 3. Selected hydrogen-bond parameters

D*—H···*A	***D*—H (Å)**	**H···*A* (Å)**	***D*···*A* (Å)**	***D*—H···*A* (°)**
Phase III, 150 K				
N3—H3A···O12^{i}	0.88	2.49	3.101 (9)	126.8
N3—H3C···O6^{ii}	0.88	2.67	3.064 (7)	108.1
N4—H4A···O1^{iii}	0.89	1.94	2.801 (7)	163.7
N4—H4B···O5	0.89	1.93	2.803 (10)	167.3
N1—H1A···O3^{iv}	0.89	1.93	2.799 (7)	164.0
N1—H1B···O8^{v}	0.89	1.91	2.789 (10)	168.4
N2—H2A···O6^{vi}	0.89	2.91	3.658 (10)	142.4
N2—H2B···O2	0.89	2.79	3.515 (12)	139.0
Phase II, 180 K				
N1—H1A···O1^{vii}	0.89	2.68	3.14 (3)	113.0
N1—H1A···O2^{viii}	0.89	2.06	2.84 (3)	145.5
N1—H1B···O1^{ix}	0.89	2.00	2.82 (3)	152.6
N1—H1B···O2^{x}	0.89	2.40	3.18 (3)	146.0
C2—H2A···O1^{xi}	0.96	2.18	3.124 (19)	169.4
N2—H2E···O2	0.91	2.67	3.20 (5)	118.2
C1—H1···O1^{xii}	0.93	2.57	3.148 (9)	120.7

Symmetrycode(s): (i) *x*, *y*-1, *z*; (ii) *x*-1, *y*, *z*; (iii) *x*-1, *y*+1, *z*-1; (iv) *x*+1, *y*, *z*; (v) *x*, *y*+1, *z*; (vi) *x*, *y*, *z*+1; (vii) -*y*+5/3, -*x*+4/3, *z*-1/6; (viii) -*x*+*y*+1, -*x*+1, *z*; (ix) -*x*+*y*+2/3, *y*-2/3, *z*-1/6; (x) -*y*+1, *x*-*y*, *z*; (xi) *x*-1/3, *x*-*y*+1/3, *z*-1/6; (xii) -*x*+*y*, -*x*+1, *z*.

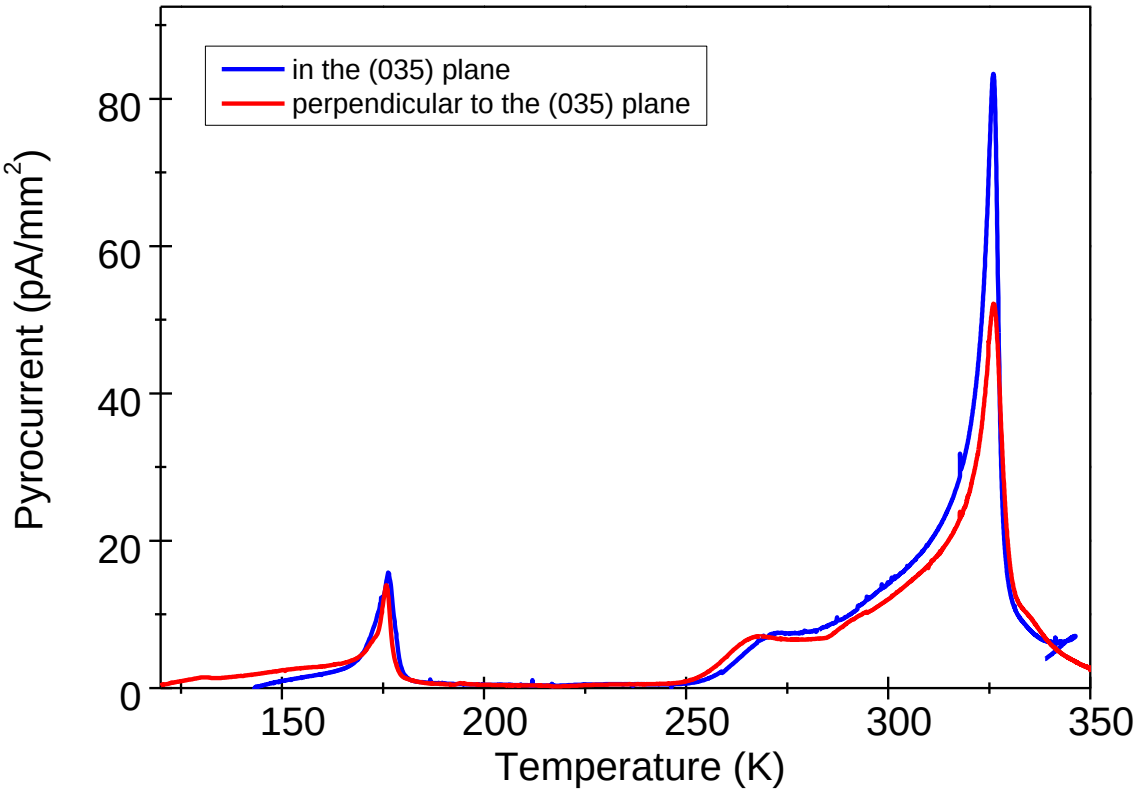

Figure S1. Temperature dependence of the pyrocurrent of **MHyZn** single crystal poled and measured in and perpendicular to the (035) plane.

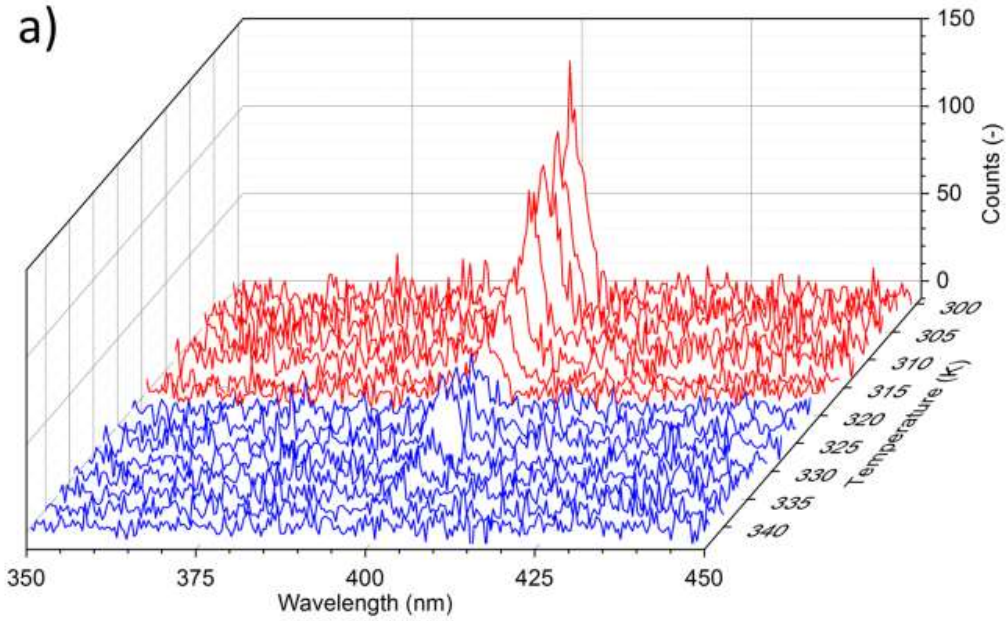

Figure S2. SHG traces for **MHyZn** collected during heating the sample from 298 to 343K. Spectra corresponding to the presence of centrosymmetric I phase are drawn in blue, while spectra corresponding to the noncentrosymmetric phase II are presented in red.

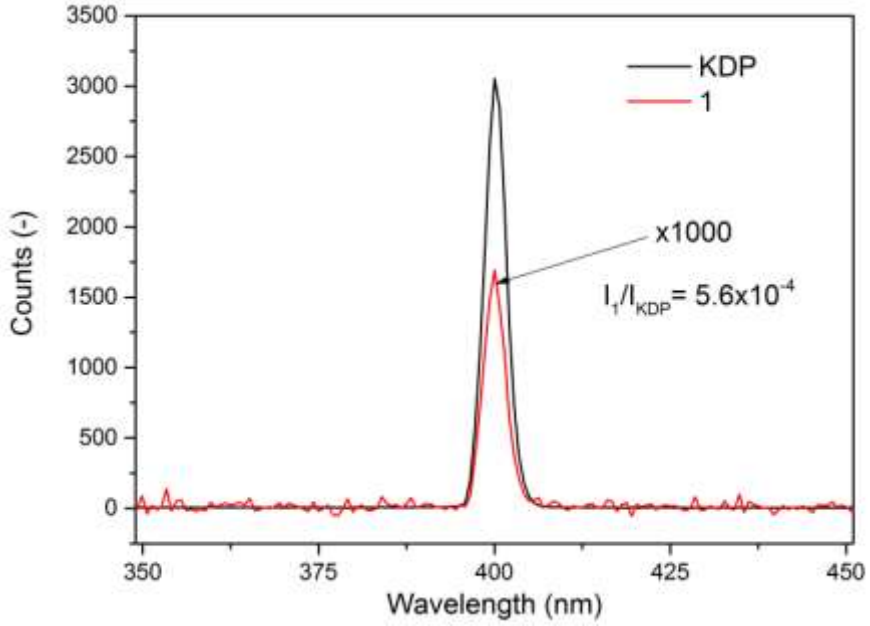

Figure S3. A comparison of averaged SHG traces for **MHyZn**(red) and that of KDP (black). Spectra are normalized to the same integration time The SHG signal produced by **MHyZn** is multiplied by 1000 to ensure the clarity of presentation of the spectrum.

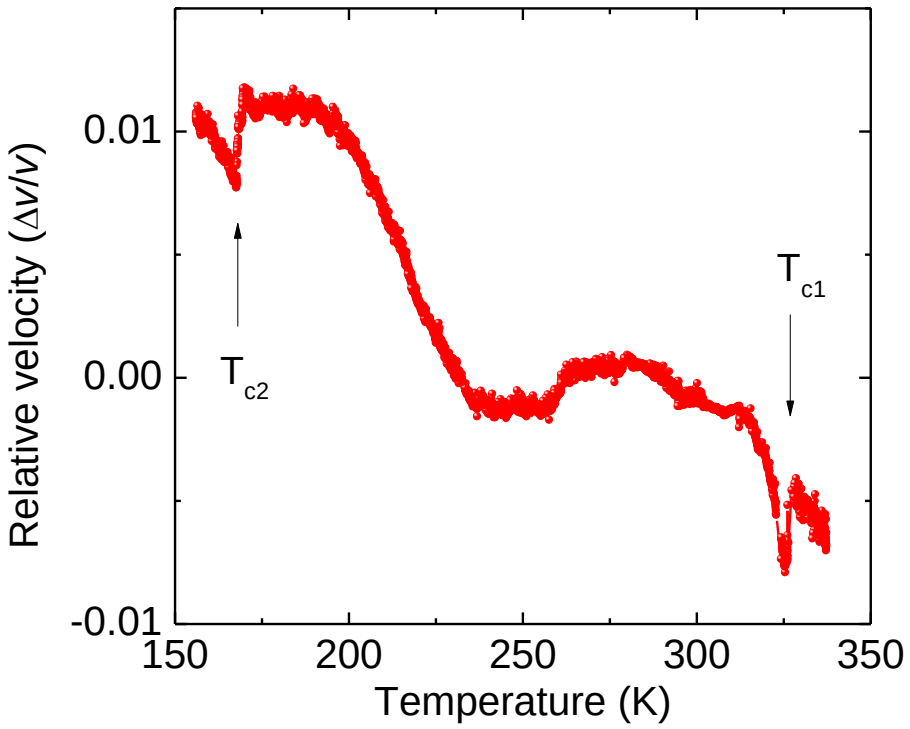

Figure S4. Temperature dependence of the ultrasonic velocity relative to the ultrasonic velocity value at room temperature. Measurements performed in the (035) plane.

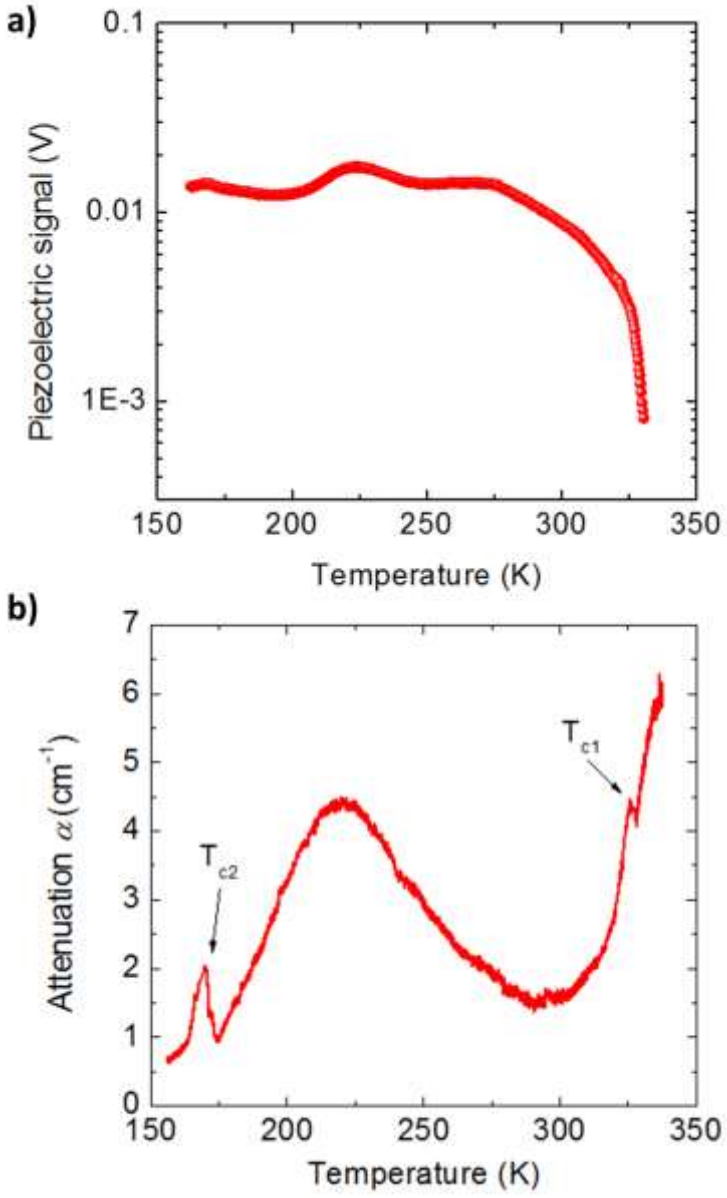

Figure S5.a)Temperature dependence of ultrasonically detected piezoelectric signal. Measurements performed along the (035) plane. b) Temperature dependence of the ultrasonic attenuation. Measurements performed in the (035) plane.

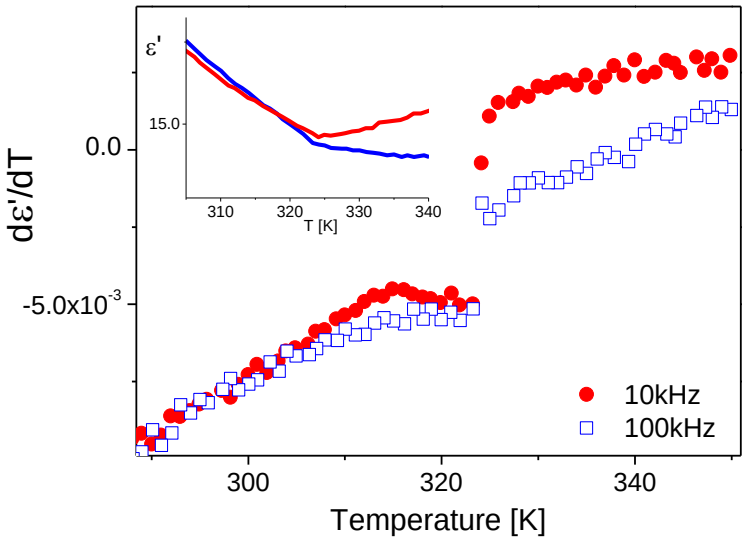

Figures S6. Temperature derivative of dielectric permittivity for two selected frequencies. The inset shows dielectric permittivitynear T_{c1}. Measurements were performed along the axis perpendicular to the (012) plane.

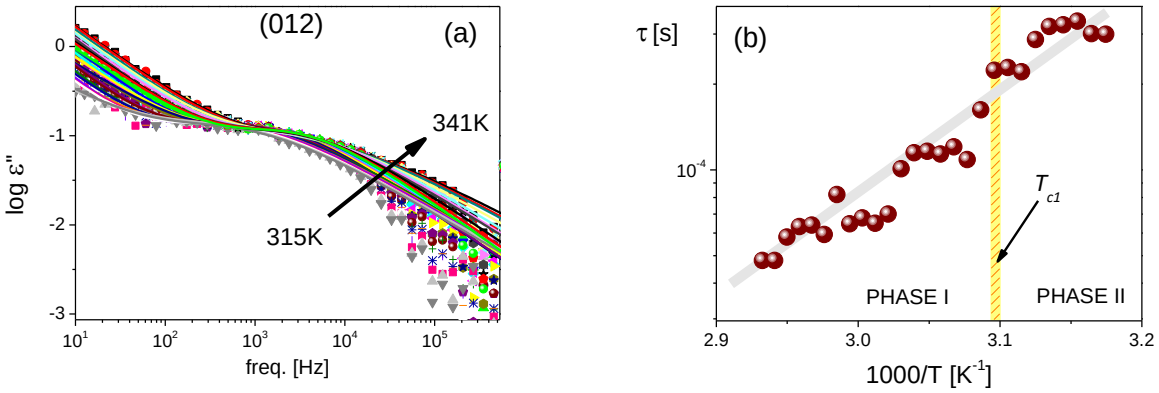

Figure S7. (a) Frequency dependence of the dielectric loss spectra in temperature range 315 – 341 K. (b) Relaxation map of high temperature dipolar relaxation process. Measurements were performed along the axis perpendicular to the (035) plane.

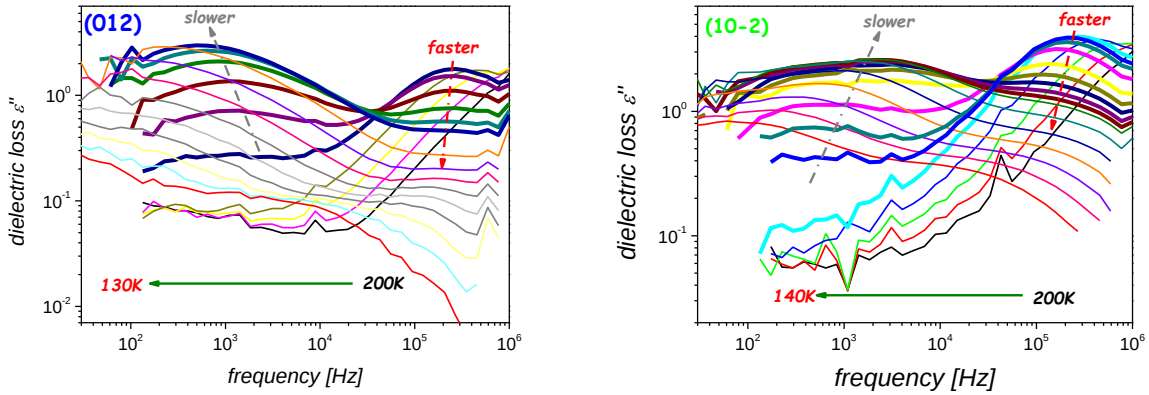

Figure S8. Frequency dependence of dielectric loss for two crystallographic direction perpendicular to the [012] and [10-2] planes in the temperature range from 130 K to 200 K.

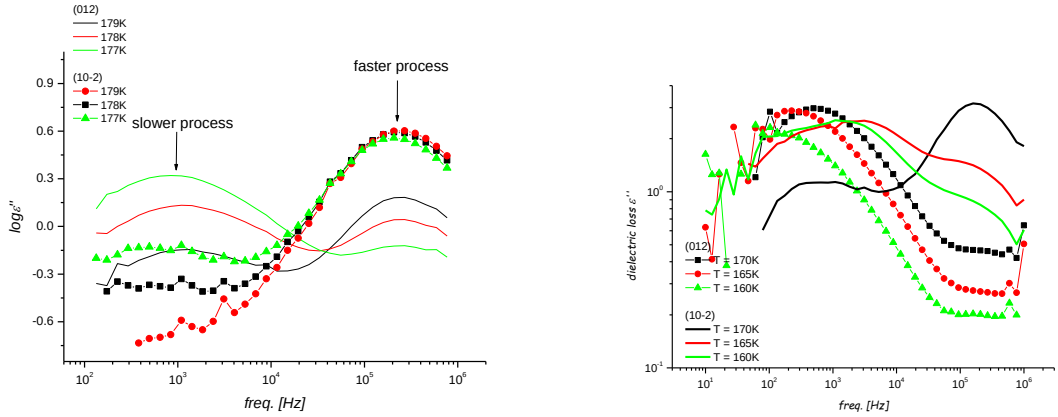

Figure S9. Comparison of the dielectric spectra measured for two different sample orientations in the vicinity of the phase transition temperature. On the left – sample oriented perpendicular to the (012), while on the right – (10-2) planes.

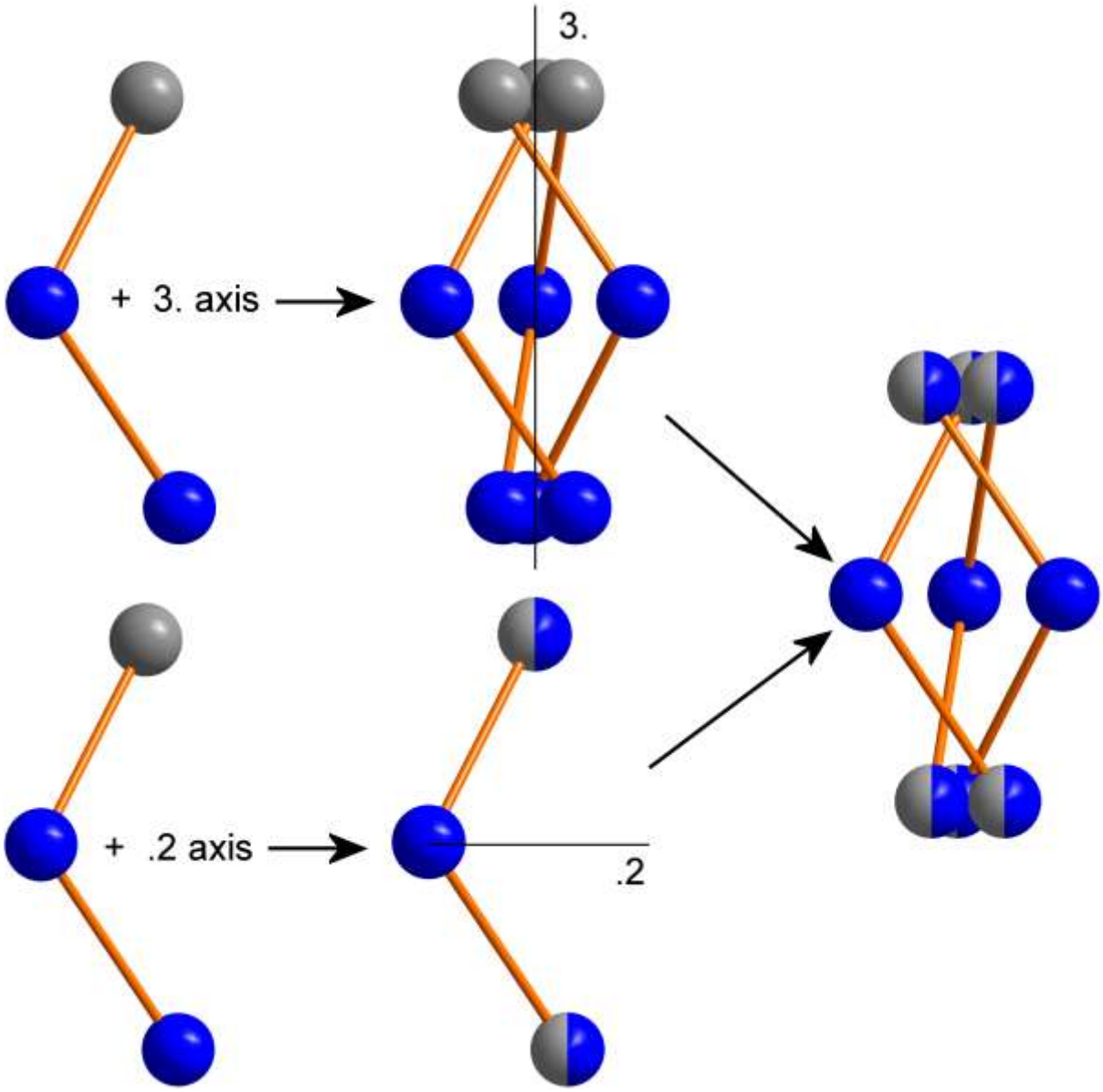

Figure S10. Possible orientation states for**MHy**$^{+}$ ions in the high-temperature phase I (R-3c symmetry).The presence of three-fold axis along the c-direction (3.) and two-fold axis in the (a,b) plane (.2) results in six various placements of **MHy**$^{+}$. In phase II only the rotations induced by the presence of 3. axis are present.